Tri-level hybrid interval-stochastic optimal scheduling for flexible residential loads under GAN-assisted multiple uncertainties☆

Xiaofei Wang [a], Fangxing Li [a,*], Jin Zhao [a], Mohammed Olama [b], Jin Dong [b], Hang Shuai [a], Teja Kuruganti [b]

[a] *The Department of Electrical Eng. & Computer Science, University of Tennessee, Knoxville, 37996, TN, USA*
[b] *Oak Ridge National Laboratory, Oak Ridge, 37830, TN, USA*

ARTICLE INFO

ABSTRACT

Various building loads, such as heating, ventilation, and air conditioners (HVACs), electric water heaters (EWHs), and electric vehicles (EVs), can introduce opportunities for improving the flexibility of electricity consumption while satisfying the needs of building owners as well as benefiting the resilience of distribution system. To utilize such flexibility, a tri-level distribution market framework is established, including residential consumers, load aggregators (LAs), and the distribution system operator (DSO). The uncertainties from all three levels are considered. The random consumption behavior at the consumer level is modeled as a Gaussian noise that is also aggregated and transmitted to the LA level. The weather temperature in the LA level is forecasted as an interval, and the photovoltaic (PV) power in the market-clearing level is modeled by a set of power scenarios generated by Generative Adversarial Networks (GANs). Then, a hybrid interval-stochastic programming is proposed to transform the uncertain problems in the first two levels into deterministic ones. For real-time implementations, a rolling horizon optimization (RHO) scheme is employed to continuously optimize the power consumption based on the latest operating information. Finally, case studies on a modified IEEE 69-bus system validate the effectiveness of the proposed uncertainty modeling strategies and the RHO scheme.

1. Introduction

Grid-interactive efficient buildings (GEBs) have been receiving wide attention in recent years. They can introduce opportunities for improving the flexibility and efficiency of electricity consumption while satisfying the needs of building owners, as well as benefiting the distribution system [1].

Buildings account for over 70 % of all U.S. electricity consumption. Among all residential loads, heating, ventilation, and air conditioners (HVACs), electric water heaters (EWHs), and electric vehicles (EVs) share most of the electricity consumption and have similar energy storage characteristics that render them high energy flexible loads [2]. Such characteristics make these building loads the research focus to satisfy grid requirements, such as load shifting, load shedding, frequency regulation, and voltage control [3,4].

On the other hand, to keep pace with the deregulation process in distribution systems, the concept of a distribution market or local market has been proposed as well as the distribution locational marginal price (DLMP) [5]. As an extension to the transmission-level locational marginal price (LMP), DLMP can reflect the physical characteristics and operating conditions of distribution systems. It can also provide price incentives for residential loads to improve their energy efficiency.

However, individual end-users do not have the capability to participate directly in the electricity market. Thus, load aggregators (LAs) are proposed as agents to aggregate a large number of residential loads to provide grid-scale services and participate in electricity markets.

Multiple studies have been conducted to aggregate individual end-users into LA. The aggregator in [6] is modeled as an intermediary to transmit load quantity and dual variables between end-users and utility. Reference [7] averages the first-order heat transfer function of all HVACs/EWHs to obtain the aggregator's heat transfer function and validate its effectiveness. The authors in [8] aggregate thermostatically controlled loads to provide synthetic inertia and primary frequency regulation services to the grid. In [9], a data generation and least-square parameter estimation (DG-LSPE) algorithm is proposed to estimate aggregator parameters for heterogeneous HVACs.

In the research community, to model the interdependence between LAs and a distribution system operator (DSO), one commonly used formulation is bilevel programming. In this formulation, LAs and the DSO are at different levels and have respective objectives. They are coupled due to the coupled variables, such as the DLMP and load quantity. In [10], LAs and the DSO are represented using a bilevel formulation with the objectives to minimize payments for LAs in the upper level and minimize the operating cost for the DSO in the lower level. References [11–13] follow a similar bilevel structure but for different types of aggregators, such as EV aggregators, virtual power plants, and microgrids. In [9], a three-layer hierarchical market structure is established to integrate the three entities: residential consumers, LAs, and the DSO. Based on these aforementioned studies, two essential enhancements can be made.

1) Uncertainties can impact system flexibility and induce unexpected economic losses. In [14,15], stochastic and robust optimizations are utilized to handle the uncertainty of renewable energy and electricity price respectively. However, only one or two uncertainty sources are considered. In a three-layer structure, uncertainties can come from multiple sources, such as renewable energies, temperature forecasts, and consumer behaviors. Thus, the appropriate modeling of these uncertainties as well as maintaining tractability are of high value.

2) As time goes by, more latest operating and forecast information are updated. Thus, the day-ahead (DA) power consumption schedule may not hold optimal. In order to benefit from the released information over time and improve the radical or conservative DA schedule, the schedule can be modified in real-time (RT).

In this context, this paper adopts our previous proposed three-layer market structure in [9], which is to minimize the total electricity cost for residential consumers as well as maintain occupant comfort and the distribution system operating constraints. Then, several enhancements and new models are proposed to address uncertainties. The detailed motivations and technical contributions can be summarized as:

- Uncertainties from all three layers and multiple sources are modeled, namely, the PV power output, outdoor temperature, and the random consumption behaviors of individual users. Especially, for the first time, the uncertainty of individual users is aggregated and transmitted to the load aggregator level.
- A feasible hybrid interval-stochastic bilevel programming model is established to simulate the interdependence of the first two levels with uncertainties, in which state-space representations and Generative Adversarial Networks (GANs) are utilized to handle the uncertainties in the first level and second level, respectively.
- A rolling horizon optimization (RHO) scheme is employed to continuously optimize the consumption schedule for consumers based on the latest operating information which makes the tri-level model schedule realistic.

The rest of this paper is organized as follows. Section 2 describes the modeling and uncertainty sources for the various residential loads. Section 3 establishes the aggregator model and the three-level optimization model. Uncertainty handling and solution methods are presented in Section 4. Section 5 introduces the RHO scheme. Case studies are performed in Section 6 to verify the proposed modeling methods and analyze the impact of uncertainties. Finally, Section 7 concludes the paper.

2. Modeling residential loads with uncertainties

In this section, the mathematical models and uncertainty sources of the various building loads are presented, including HVACs, EWHs, and EVs.

2.1. HVAC model

An HVAC maintains the room temperature through a thermostat. The first-order thermal transfer function is utilized to model a building's varied indoor temperature [16]. However, the indoor temperature may not strictly follow this heat transfer function due to the inherent inaccuracy and householder's random behaviors, e.g., opening windows, cooking, having guests in the house, etc. To account for such uncertainties, a Gaussian noise is added to the original HVAC model. Without loss of generality, we consider a cooling HVAC mode in this study. Then, each HVAC can be modeled with the following expressions:

$$\theta_{i,j,t+1}^h = a_{i,j}^h \theta_{i,j,t}^h + b_{i,j}^h \widetilde{\theta}_t^{out} + g_{i,j}^h u_{i,j,t}^h + \widetilde{\varepsilon}_{i,j,t}^h \tag{1}$$

$$\theta^{h,\min} \leqslant \theta_{i,j,t}^h \leqslant \theta^{h,\max} \tag{2}$$

where $\theta_{i,j,t}^h$ is the indoor temperature of building j in aggregator i at time t; $\widetilde{\theta}_t^{out}$ is the forecasted outdoor temperature; $u_{i,j,t}^h$ is the ON/OFF status of HVAC j at time t; $\widetilde{\varepsilon}_{i,j,t}^h$ is the Gaussian noise, $\widetilde{\varepsilon}_{i,j,t}^h \sim N\left(0, \left(\alpha^h \theta^{h,mid}\right)^2\right)$, $\theta^{h,mid} = \left(\theta^{h,\min} + \theta^{h,\max}\right)/2$, α^h is a scaler to control the uncertainty level; $a_{i,j}^h$, $b_{i,j}^h$, and $g_{i,j}^h$ are the coefficients of the thermal function of HVAC j; $\theta^{h,\min}$ and $\theta^{h,\max}$ are the consumer's preferable temperature boundaries. The typical parameters of a single HVAC can be found in [9].

2.2. EWH model

For an EWH, the uncertainty is the forecasted water usage. Then, similar to HVAC, each EWH can be represented as:

$$\theta_{i,j,t+1}^w = a_{i,j}^w \theta_{i,j,t}^w - b_{i,j}^w \widetilde{W}_{i,j,t}^D + g_{i,j}^w u_{i,j,t}^w + c_{i,j}^w \tag{3}$$

$$\theta^{w,\min} \leqslant \theta_{i,j,t}^w \leqslant \theta^{w,\max} \tag{4}$$

where $\theta_{i,j,t}^w$ is the water temperature in the water tank; $b_{i,j}^w$ represents the temperature drop when consuming 1-liter hot water; $g_{i,j}^w$ is the water temperature rise after heating 1 hour; $u_{i,j,t}^w$ is the ON/OFF status of the EWH; $\widetilde{W}_{i,j,t}^D \sim N\left(\overline{W}_{i,j,t}^D, \left(\alpha^w \overline{W}_{i,j,t}^D\right)^2\right)$, $\overline{W}_{i,j,t}^D$ is the forecasted water usage at time t, α^w is a scaler. The derivation of these parameters can be found in the Appendix.

2.3. EV model

For an EV, the uncertainty is the forecasted daily driving distance. Then, the state-of-charge (SOC) of an EV can be presented as:

$$E_{i,j,t+1} = E_{i,j,t} - P_{i,j,t}^c/\sqrt{\eta_i} + \sqrt{\eta_i} P_{i,j,t}^{dri} \tag{5}$$

$$SOC^{E,\min} \cdot E_{i,j}^r \leqslant E_{i,j,t+1} \leqslant SOC^{E,\max} \cdot E_{i,j}^r \tag{6}$$

$$\sum_{t=1}^{T} P_{i,j,t}^{dri} = e^d \cdot \widetilde{d}_{i,j} \tag{7}$$

where $E_{i,j,t}$ is the stored energy of EV j in aggregator i; $P_{i,j,t}^c$ is the charging power; $P_{i,j,t}^{dri}$ is the driving consumption power; η_i is the round-

trip efficiency; $E_{i,j}^r$ is the rated energy of EV j; $SOC^{E,min}$ and $SOC^{E,max}$ are the consumer's preferable SOC boundaries; e^d is the driving energy consumption per mile, $\tilde{d}_{i,j} \sim N\left(\overline{d}_{i,j}, \left(\alpha^e \overline{d}_{i,j}\right)^2\right)$, $\overline{d}_{i,j}$ is the forecasted daily driving distance, α^e is a scaler. The typical parameters of a single EV can be found in [9].

3. Day-Ahead: Tri-Level market framework

In this section, a tri-level market framework is established to represent the relationship between residential consumers, LAs, and the DSO. In this structure, each entity has its objective and operating constraints which are considered separately. The LA collects all operation and preference information from the contracted residential users. Then, the aggregated model is established and the LA bids in the distribution market. After collecting bids and offers from all market participants, the DSO clears the market and broadcasts generation/load capacity and DLMP to all participants. At last, the LAs dispatch the optimal aggregated loads to end-users.

3.1. First Level: LAs

The first level minimizes the total electricity payments for LAs which include HVAC aggregator, EWH aggregator, and EV aggregator.

$$\min \sum_{t \in T} \left(\sum_{i \in H} \pi_{i,t}^p \cdot P_{i,t}^H + \sum_{i \in W} \pi_{i,t}^p \cdot P_{i,t}^W + \sum_{i \in E} \pi_{i,t}^p \cdot P_{i,t}^C \right) \tag{8}$$

where $\pi_{i,t}^p$ is the DLMP; $P_{i,t}^H$, $P_{i,t}^W$ and $P_{i,t}^C$ are respectively the power consumption of HVAC, EWH and EV aggregators; H, W and E are the set of aggregators, T is the set the simlation time slots.

1) HVAC aggregator model: By utilizing the DG-LSPE algorithm proposed in [9], the HVAC aggregator's thermal transfer function in a cooling mode can be obtained. The operating constraints are shown below, the uncertainties are the forecasted outdoor temperature $\tilde{\theta}_t^{out}$ and the aggregated noise $\tilde{\varepsilon}_{i,t}^h$.

$$\theta_{i,t+1}^h = a_i^h \theta_{i,t}^h + b_i^h \tilde{\theta}_t^{out} + g_i^h u_{i,t}^h + \tilde{\varepsilon}_{i,t}^h \tag{9}$$

$$\theta^{h,min} \leqslant \theta_{i,t}^h \leqslant \theta^{h,max} \tag{10}$$

$$syn_i^{h,min} \leqslant u_{i,t}^h \leqslant syn_i^{h,max} \tag{11}$$

$$-\Delta u_i^{h,dr} \leqslant u_{i,t+1}^h - u_{i,t}^h \leqslant \Delta u_i^{h,ur} \tag{12}$$

$$SOC_{i,t}^h = \frac{\theta^{h,max} - \theta_{i,t}^h}{\theta^{h,max} - \theta^{h,min}} \tag{13}$$

$$SOC_i^{h,min} \leqslant SOC_{i,t}^h \leqslant SOC_i^{h,max} \tag{14}$$

$$P_{i,t}^H = u_{i,t}^h \cdot N_i^h \cdot P^{h,rated} \tag{15}$$

$$\tilde{\theta}_t^{out} \in \left[\underline{\theta}_t^{out}, \overline{\theta}_t^{out}\right] = \left[\theta_t^{out} - \alpha^{temp}\theta_t^{out}, \theta_t^{out} + \alpha^{temp}\theta_t^{out}\right] \tag{16}$$

where (9) represents the varied indoor temperature; $\theta_{i,t}^h$ is the indoor temperature of aggregator i at time t; a_i^h, b_i^h and g_i^h are the coefficients of the aggregator; $u_{i,t}^h$ is an approximate continuous variable in [0, 1] indicating the ON status ratio in HVAC aggregator i; $\tilde{\varepsilon}_{i,t}^h$ is the aggregated noise of end users, $\tilde{\varepsilon}_{i,t}^h \sim N\left(0, \sigma_{i,t}^{h2}\right)$, $\sigma_{i,t}^h = \sqrt{\sum_{j=1}^{N_i^h} \left(\alpha^h \theta^{mid}\right)^2}/N_i^h$, N_i^h is the number of HVACs in aggregator i; (10) is the indoor temperature setting boundary; (11) is the synchronous constraint which limits the number of HVACs to be turned ON at time step t; (12) is the ramp constraints to limit the status transformation rate; (13) and (14) are energy constraints to avoid the situation that indoor temperatures centering at the setting

temperature boundaries [17]; (15) is to obtain the active power of the HVAC aggregator; (16) is the outdoor temperature forecasting interval; and α^{temp} is a scaler to control the uncertainty interval.

2) EWH aggregator model: Similar to the HVAC aggregator model, the EWH aggregator model and operating constraints are shown as follows:

$$\theta_{i,t+1}^w = a_i^w \theta_{i,t}^w - b_i^w \tilde{W}_{i,t}^D + g_i^w u_{i,t}^w + c_i^w \tag{17}$$

$$\theta^{w,min} \leqslant \theta_{i,t}^w \leqslant \theta^{w,max} \tag{18}$$

$$syn_i^{w,min} \leqslant u_{i,t}^w \leqslant syn_i^{w,max} \tag{19}$$

$$-\Delta u_i^{w,dr} \leqslant u_{i,t+1}^w - u_{i,t}^w \leqslant \Delta u_i^{w,ur} \tag{20}$$

$$SOC_{i,t}^w = \frac{\theta^{w,max} - \theta_{i,t}^w}{\theta^{w,max} - \theta^{w,min}} \tag{21}$$

$$SOC_i^{w,min} \leqslant SOC_{i,t}^w \leqslant SOC_i^{w,max} \tag{22}$$

$$P_{i,t}^W = u_{i,t}^w \cdot N_i^w \cdot P^{w,rated} \tag{23}$$

where the aggregated coefficients a_i^w, b_i^w, g_i^w and c_i^w can also be obtained by the DG-LSPE algorithm; the uncertainty is the aggregated water usage $\tilde{W}_{i,t}^D$, $\tilde{W}_{i,t}^D \sim N\left(\overline{W}_{i,t}^D, \sigma_{i,t}^{w2}\right)$, $\overline{W}_{i,t}^D = \sum_{j=1}^{N_i^w} \overline{W}_{i,j,t}^D/N_i^w$, $\sigma_{i,t}^w = \sqrt{\sum_{j=1}^{N_i^w} \left(\alpha^w \overline{W}_{i,j,t}^D\right)^2}/N_i^w$, and N_i^w is the number of EWHs in aggregator i.

3) EV aggregator model: The EV aggregator and operating constraints can be modeled as:

$$E_{i,t+1} = E_{i,t} + \sqrt{\eta_i} P_{i,t}^C - P_{i,t}^{Dri}/\sqrt{\eta_i} \tag{24}$$

$$SOC_i^{e,min} \cdot E_i^R \leqslant E_{i,t+1} \leqslant SOC_i^{e,max} \cdot E_i^R \tag{25}$$

$$0 \leqslant P_{i,t}^C \leqslant P_i^{C,max} \tag{26}$$

$$E_{i,t=0} \leqslant E_{i,t=T} \tag{27}$$

$$\sum_{t=1}^T P_{i,t}^{Dri} = e^d \tilde{d}_i \tag{28}$$

$$E_i^R = \sum_j^{N_i^e} E_{i,j}^r \tag{29}$$

where (24) is the energy of EV aggregator i; it is assumed all EVs have the same round-trip efficiency η_i; (25) represents the aggregator's SOC limits; (26) is the charging power limit; (27) ensures the total charging energy is no less than the total consumption energy; (28) describes the driving consumption power; (29) refers to the rated energy of an aggregator which equals to the summation of the rated energy of multiple EVs, the uncertainty is the aggregated daily driving distance $\tilde{d}_i$, $\tilde{d}_i \sim N\left(\overline{d}_i, \sigma_i^{e2}\right)$, $\overline{d}_i = \sum_{j=1}^{N_i^e} \overline{d}_{i,j}$, and $\sigma_i^e = \sqrt{\sum_{j=1}^{N_i^e} \left(\alpha^e \overline{d}_{i,j}\right)^2}$.

3.2. Second Level: DSO

In the second level, the DSO clears the market, its objective is to minimize the system's generation cost. The uncertainty is PV's power output $\tilde{P}_{i,t}^{PV}$.

$$\min \sum_{t \in T} \sum_{i \in G} c_{i,t} \cdot P_{i,t}^G \tag{30}$$

s.t.

$$\sum_{i \in G} P_{i,t}^G + \sum_{i \in PV} \widetilde{P}_{i,t}^{PV} = \sum_{i \in B} P_{i,t}^D + \sum_{i \in H} P_{i,t}^H + \sum_{i \in W} P_{i,t}^W + \sum_{i \in E} P_{i,t}^C + P_t^{loss} : \lambda_t^p \tag{31}$$

$$\sum_{i \in G} Q_{i,t}^G = \sum_{i \in B} Q_{i,t}^D + Q_t^{loss} : \lambda_t^q \tag{32}$$

$$V^{\min} \leqslant V_{sub,t} + \sum_{i \in B} Z_{j,i}^p \left(P_{i,t}^G + \widetilde{P}_{i,t}^{PV} - P_{i,t}^D - P_{i,t}^H - P_{i,t}^W - P_{i,t}^C \right) + \\ \sum_{i \in B} Z_{j,i}^q \left(Q_{i,t}^G - Q_{i,t}^D \right) \leqslant V^{\max} : \omega_{j,t}^{v,\min}, \omega_{j,t}^{v,\max} \tag{33}$$

$$P_{i,t}^{G,\min} \leqslant P_{i,t}^G \leqslant P_{i,t}^{G,\max} : \omega_{i,t}^{p,\min}, \omega_{i,t}^{p,\max} \tag{34}$$

$$Q_{i,t}^{G,\min} \leqslant Q_{i,t}^G \leqslant Q_{i,t}^{G,\max} : \omega_{i,t}^{q,\min}, \omega_{i,t}^{q,\max} \tag{35}$$

$$\pi_{i,t}^p = \frac{\partial L}{\partial P_{i,t}^D} = \lambda_t^p + \left(\lambda_t^p \cdot \frac{\partial P_t^{loss}}{\partial P_{i,t}^D} + \lambda_t^q \cdot \frac{\partial Q_t^{loss}}{\partial P_{i,t}^D} \right) + \sum_{j \in B} \left(\omega_{j,t}^{v,\min} - \omega_{j,t}^{v,\max} \right) Z_{j,i}^p \tag{36}$$

where (31) and (32) are the active and reactive power balance constraints; $P_{i,t}^G$, $P_{i,t}^D$, $P_{i,t}^H$, $P_{i,t}^W$, $P_{i,t}^C$, P_t^{loss}, $Q_{i,t}^G$, $Q_{i,t}^D$, and Q_t^{loss} are the active/reactive generation/load/power loss respectively; (33) represents the voltage limit which is derived from linearized power flow for distribution (LPF-D) [5]; Z^p and Z^q are matrices of nodal voltage change to net power injections, where the substation is the reference bus that connects to the transmission system; (34) and (35) are generators' active and reactive power output limits; (36) is the expression of the DLMP which is derived from the Lagrangian function of the second level problem, it can be seen that the DLMP includes three components: the marginal energy price, the marginal loss price (including real and reactive power), and the marginal voltage support price; λ_t^p, λ_t^q, $\omega_{j,t}^{v,\min}$, $\omega_{j,t}^{v,\max}$, $\omega_{i,t}^{p,\min}$, $\omega_{i,t}^{p,\max}$, $\omega_{i,t}^{q,\min}$ and $\omega_{i,t}^{q,\max}$ are dual variables. The power loss is linearized by using the first order Taylor's series.

$$P_t^{loss} \approx P_t^{loss*} + \sum_{i \in B} \frac{\partial P_t^{loss}}{\partial P_{i,t}^G} \left(\Delta P_{i,t}^G - \Delta P_{i,t}^D \right) + \sum_{i \in B} \frac{\partial P_t^{loss}}{\partial Q_{i,t}^G} \left(\Delta Q_{i,t}^G - \Delta Q_{i,t}^D \right) \tag{37}$$

$$Q_t^{loss} \approx Q_t^{loss*} + \sum_{i \in B} \frac{\partial Q_t^{loss}}{\partial P_{i,t}^G} \left(\Delta P_{i,t}^G - \Delta P_{i,t}^D \right) + \sum_{i \in B} \frac{\partial Q_t^{loss}}{\partial Q_{i,t}^G} \left(\Delta Q_{i,t}^G - \Delta Q_{i,t}^D \right) \tag{38}$$

where power losses P_t^{loss*} and Q_t^{loss*}, power output $P_{i,t}^{G*}$ and $Q_{i,t}^{G*}$, and load demand $P_{i,t}^{D*}$ and $Q_{i,t}^{D*}$ refer to the power flow results at an initial operating point; $\frac{\partial P_t^{loss}}{\partial P_{i,t}^G}$ and $\frac{\partial P_t^{loss}}{\partial Q_{i,t}^G}$ are the partial derivatives of P_t^{loss} to bus injection $P_{i,t}^G$ and $Q_{i,t}^G$ at every bus and every time step, and they are opposite in sign with the partial derivatives of P_t^{loss} to bus demand $P_{i,t}^D$ and $Q_{i,t}^D$; $\Delta P_{i,t}^G = P_{i,t}^G - P_{i,t}^{G*}$ is the power difference between the to-be-determined operating point and the initial operating point; $\Delta Q_{i,t}^G$, $\Delta P_{i,t}^D$ and $\Delta Q_{i,t}^D$ can be expressed similarly.

The related linearization discussion can also be found in [5]. The main difference between [5] and this work is that P^D and Q^D are assumed constant in the former but considered flexible loads in this work. So $\Delta P_{i,t}^D = P_{i,t}^D - P_{i,t}^{D*}$ is also one item in (37).

3.3. Third Level: Individual end users

In the third level, each LA dispatches the corresponding optimal load obtained in the first level to individual end-users. The priority-control-based load dispatching algorithm for HVACs, EWHs, and EVs in [9] is used in this study for dispatching the end-users.

4. Uncertainty modeling and solution methods

The proposed trilevel problem with uncertainties in each level is hard to solve directly. Thus, two methods are applied to transform the original problem into a tractable one. 1) Decoupling: the first two levels are within a bilevel structure, and they have a leader–follower structure with the third level. Thus, the trilevel problem can be decoupled and solved sequentially, which means the first two levels are solved first, then the optimal aggregated load is dispatched to individual consumers in the third level. 2) Uncertainty handling: to solve the bilevel problem with uncertainties, the first step is to transform the uncertainty models into the equivalent deterministic ones by interval or stochastic optimization. Then, the mature bilevel solution methods can be used to solve the deterministic bilevel problems.

4.1. Uncertainty handling

Interval optimization and stochastic programming are the two widely used uncertainty handling methods. How to handle uncertainties to ensure the solvability and maintain decision-maker's objective is a key point. In this paper, in the first level, interval optimization is utilized to model the uncertainty of the forecasted temperature and the aggregated random power consumption behaviors to obtain the best and worst payment for aggregators. In the second level, stochastic programming is adopted to simulate the volatility of PV power output.

There are three considerations for these different handling strategies. 1) From the perspective of LAs in the first level, they may care more about the best and worst payment range rather than the expected payment, thus interval optimization is appropriate. 2) Based on the available PV historical data, possible PV scenarios can be generated, then stochastic modeling is more effective as a risk measure [18]. 3) Another advantage is that stochastic programming can maintain the convexity of the second level which ensures the bilevel problem is tractable.

1) Uncertainty transformation in the first level: State-space representation

The variable $\theta_{i,t}^h$ in (9) is a time-dependent variable, thus the state-space structure is proper to represent the dependent relationship. Constraint (9) can be written as below:

$$\boldsymbol{\theta} = \boldsymbol{A}^{-1} \left(\boldsymbol{B} \widetilde{\boldsymbol{\theta}}^{out} + \boldsymbol{G}\boldsymbol{u} + \boldsymbol{C} + \widetilde{\boldsymbol{\varepsilon}} \right) \tag{39}$$

where $\boldsymbol{A}$ is a diagonal matrix with diagonal elements 1 and sub-diagonal elements -a; $\boldsymbol{B}$ and $\boldsymbol{G}$ are diagonal matrices with diagonal elements b and g respectively; $\boldsymbol{C}$ is the vector with initial conditions, and $\boldsymbol{C}$ = $[a\theta_0, 0, ..., 0]^T$. By setting 95% confidence interval, the uncertainty interval is $\widetilde{\boldsymbol{\varepsilon}} \in [-2\boldsymbol{\sigma}, 2\boldsymbol{\sigma}]$. Note that (39) is a general formulation of the indoor temperature for each HVAC aggregator.

Next, by merging constraints (9) and (10), we have:

$$\boldsymbol{\theta}^{\min} \leqslant \boldsymbol{A}^{-1} \left(\boldsymbol{B} \widetilde{\boldsymbol{\theta}}^{out} + \boldsymbol{G}\boldsymbol{u} + \boldsymbol{C} + \widetilde{\boldsymbol{\varepsilon}} \right) \leqslant \boldsymbol{\theta}^{\max} \tag{40}$$

The interval optimization model can be converted to an optimistic model and a pessimistic model [19]. The robust counterpart for the optimistic model is:

$$\boldsymbol{A}^{-1} \left(\boldsymbol{B}\underline{\boldsymbol{\theta}}_{out} + \boldsymbol{G}\boldsymbol{u} + \boldsymbol{C} + \underline{\boldsymbol{\varepsilon}} \right) \leqslant \boldsymbol{\theta}^{\max} \tag{41}$$

$$\boldsymbol{\theta}^{\min} \leqslant \boldsymbol{A}^{-1} \left(\boldsymbol{B}\overline{\boldsymbol{\theta}}_{out} + \boldsymbol{G}\boldsymbol{u} + \boldsymbol{C} + \overline{\boldsymbol{\varepsilon}} \right) \tag{42}$$

While the robust counterpart for the pessimistic model is:

$$\boldsymbol{A}^{-1} \left(\boldsymbol{B}\overline{\boldsymbol{\theta}}_{out} + \boldsymbol{G}\boldsymbol{u} + \boldsymbol{C} + \overline{\boldsymbol{\varepsilon}} \right) \leqslant \boldsymbol{\theta}^{\max} \tag{43}$$

$$\boldsymbol{\theta}^{\min} \leqslant \boldsymbol{A}^{-1} \left(\boldsymbol{B}\underline{\boldsymbol{\theta}}_{out} + \boldsymbol{G}\boldsymbol{u} + \boldsymbol{C} + \underline{\boldsymbol{\varepsilon}} \right) \tag{44}$$

Constraints (13) and (14) can be merged in the same way.

The state-space representation for EWHs and EVs can also be obtained in a similar way. Now, the uncertainties in the first level have been transformed into deterministic ones.
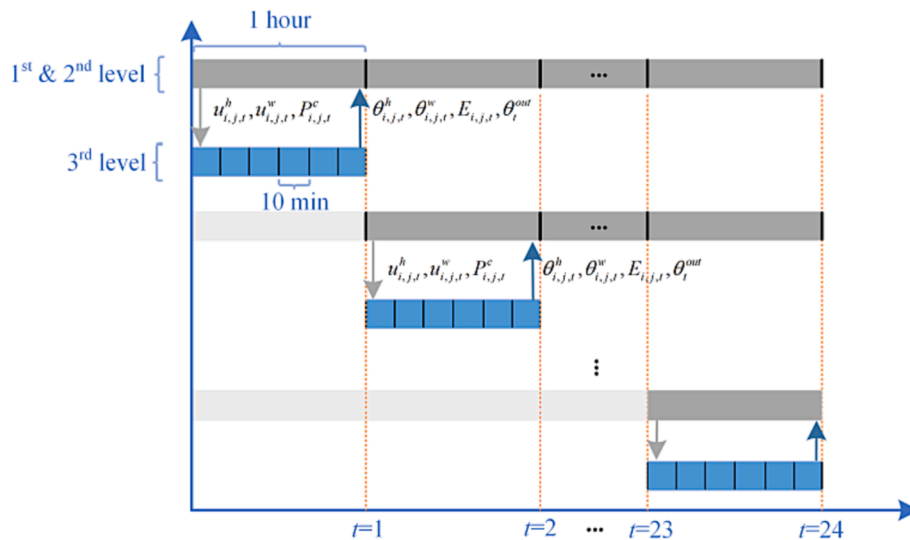
Fig. 1. Illustration of the rolling horizon optimization scheme.

2) Uncertainty transformation in the second level: GANs scenario generation

To simulate the uncertainty of PV power output, a widely used approach is to generate a finite number of possible PV scenarios. Then, the second level becomes a stochastic programming problem.

In addition to the traditional probability-based scenario generation methods, a series of machine learning related methods have been proposed in power systems in recent years. In [20], the k-means, as an unsupervised learning method, is utilized to classify the historical data and reduce the number of the generated scenarios. In [21], the long short-term memory (LSTM) is proposed to characterize the stochasticity of the electricity price. GANs have been extended to generate power scenarios for renewable resources in [22]. Compared to the traditional methods, GANs have two advantages: 1) they can generate scenarios only according to historical data, without assuming or fitting probability distributions; 2) they belong to unsupervised learning, which can avoid labeling work that sometimes is impossible and inaccurate. Thus, the GANs approach is selected for scenario generation in this study.

The detailed scenario generation procedures are elaborated in [22]. These huge number of generated scenarios cover most if not all possible PV outputs. However, only a fraction of scenarios has a similar pattern with the day-ahead PV point-forecast power. Based on all scenarios and the forecasted power, a candidate scenario set can be obtained, and then a scenario reduction strategy is introduced to reduce the computational burden.

The main idea of scenario reduction is to minimize the Kantorovich probability distance between reduced scenarios and the candidate scenario set. The detailed mathematical derivations can be found in [23]. The procedures of obtaining the candidate scenario set and scenarios reduction are illustrated in Algorithm 1.

Algorithm 1: Scenario Reduction

1. Initialization: Calculate the Euclidean distance between point forecast profile and all scenarios;

$$d(\overline{\boldsymbol{P}}^{PV}, \boldsymbol{P}^{PV,s}) = \left\| \overline{\boldsymbol{P}}^{PV} - \boldsymbol{P}^{PV,s} \right\|_2, \quad s = 1, 2, ..., S$$

where $\overline{\boldsymbol{P}}^{PV}$ is the point-forecast power, and $\boldsymbol{P}^{PV,s}$ is the generated scenario.

2. Candidate Scenario set: Choose the closest 30 % of all scenarios as the candidate scenario set S_C, with the probability of each candidate scenario $p = 1/|S_C|$;

3. Kantorovich probability distance-based scenario reduction:

   3.1 Eliminate scenario s_m if it meets the following condition;

     $d_m = \min \left\{ p(m) \cdot p(n) \cdot d(\boldsymbol{P}^{PV,m}, \boldsymbol{P}^{PV,n}) \right\} \; m, n \in \{1, ..., S_C\}, n \neq m$

   3.2 Update the probability of s_n and the number of scenarios;

     $S_C = S_C - 1, \; p(n) = p(n) + p(m)$

   3.3 If $S_C > S_0$ (S_0 is the preferred scenario number), go back to **Step 3.1**; otherwise, terminate the algorithm.

---

3) Compact notation

Based on the uncertainty modeling, the unified compact notation of the first two levels for the optimistic model or the pessimistic model can be presented as follows [24]:

$$\min_{\boldsymbol{y}} \sum_{s \in S_0} p(s) \boldsymbol{\pi}^T(s) \boldsymbol{y} \tag{45}$$

$$s.t. \quad \boldsymbol{Ay} \leqslant \boldsymbol{b} \tag{46}$$

$$\boldsymbol{\pi}(s) \in \arg\min_{\boldsymbol{x}} \sum_{s \in S_0} p(s) \boldsymbol{c}^T \boldsymbol{x}(s) \tag{47}$$

$$s.t. \quad \boldsymbol{W}(s)\boldsymbol{x}(s) \leqslant \boldsymbol{r}(s) - \boldsymbol{T}(s)\boldsymbol{y} \tag{48}$$

where (45)-(46) represent the objective and constraints of the optimistic model or the pessimistic model in the first level, and (47)-(48) represent the stochastic model in the second level.

4.2. Solution method

The solution methods of the bilevel problem have been widely studied [25]. In this paper, due to the convexity in the second level, the equivalent transformation via Karush-Kuhn-Tucker (KKT) optimal conditions is adopted. The coupled first two levels can be solved into two steps which are presented below.

1) Mathematical program with equilibrium constraints (MPEC) model: The second level is a deterministic linear programming problem with a finite number of scenarios, it can be transformed into a set of constraints adding to the first level by obtaining the KKT optimality conditions. Then, the bilevel problem becomes a single-level problem which is called MPEC.

2) Mixed-integer linear programming (MILP) model: The MPEC model is non-convex due to the bilinear objective function and the complementary slackness constraints. Therefore, the strong duality theory and big-M approach can be utilized to transform the MPEC to a MILP which is tractable. The detailed derivation of MPEC and MILP can be found in [26] and is neglected here.

5. Real-Time: Rolling horizon optimization

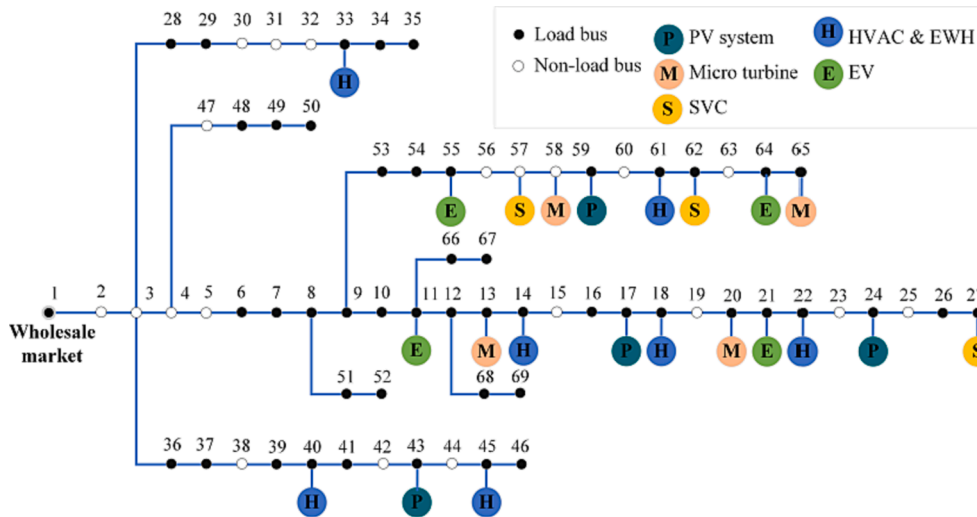In this section, to reflect the continuous clearing nature of the RT

Fig. 2. The modified IEEE 69-bus system.

market and integrate the latest operating information, RHO is applied to allow the re-scheduling and re-dispatching [27].

In general, the closer to the real-time t, the less prediction errors of the PV power output and outdoor temperature, and the more accurate end users' housing/EV conditions. In this context, aggregators are willing to adjust their schedules and the DSO can make a precise DA market clearing. By incorporating the latest released information, the radicalness and conservativeness of the interval optimization in the DA market can also be reduced.

The diagram of the RHO scheme is illustrated in Fig. 1. The procedures of the RHO scheme are described in Algorithm 2. The first two levels are highly coupled due to the coupled decision variables: Utilizing fewer data is indeed an advantage for some methods. They form a Stackelberg model: LAs bid in the distribution market with load demands, DSO clears the market and sends the DLMP back to LAs, then LAs make their decisions based on DLMP and resubmit their bids, and so on. The complicated process in these two levels can be solved by the typical bilevel solution described in Section 4.2. After that, LAs can obtain the aggregated demand $P_{i,t}^H$, $P_{i,t}^W$ and $P_{i,t}^C$. As shown in Fig. 1, the time step in the first two levels is 1 h, while the third level utilizes a high-resolution control interval which is 10 min. In the third level, LAs dispatch the aggregated demand to all the contracted consumers based on the priority-based dispatching algorithm. LAs send control signals (e.g., $u_{i,j,t}^h$, $u_{i,j,t}^w$, $P_{i,j,t}^c$) to consumers at the beginning of every 10 min, collect operating information (e.g., $\theta_{i,j,t}^h$, $\theta_{i,j,t}^w$, $E_{i,j,t}$, $\widetilde{\theta}_t^{out}$) at the end of every 10 min, and calculate the control signals and resend them to consumers for the next 10 min. At the end of the 1-hour time step, LAs update $\theta_{i,t+1}^h$, $\theta_{i,t+1}^w$, $E_{i,t+1}$, and $\widetilde{\theta}_{t+1}^{out}$ for the next RHO schedule.

Algorithm 2: Procedures of RHO

---

1. **Aggregator level**: At t, LAs collect the forecasted outdoor temperature $\widetilde{\theta}_t^{out}$ and indoor temperatures $\theta_{i,j,t}^h$, water temperatures $\theta_{i,j,t}^w$, EV SOCs of individual users, then update the aggregated indoor temperature $\theta_{i,t}^h$, water temperature $\theta_{i,t}^w$ and EV energy $E_{i,t}$;
2. **DSO level**: The DSO collects the latest forecasted PV power output, then updates the PV power scenarios by Algorithm 1;
3. **Solve the first bi-level model:** Solve the rest (24 - t) hours interval-stochastic bi-level model, obtain the optimal load demand schedule, the time step is 1 h;
4. **Residential level:** LAs dispatch the optimal demand schedule of hour $t + 1$ to individual users;
5. **Termination checking:** $t = t + 1$, check whether $t <= T$ or not. If yes, go back to **Step 1**; otherwise, the algorithm terminates.

Table 1
Parameters of the modified IEEE 69-bus system.

Class	Parameter	Typical Value
MT	Location	Bus #13, 20, 58, 65
	Bidding price	$ 70/MWh
	Capacity	0.5 MW
	α_i	0.95
SVC	Location	Bus #27, 57, 62
	Bidding price	$ 0/MVarh
	Capacity	0.5 MVar
PV	Location	Bus #17, 24, 43, 59
	Bidding price	$ 15/MWh
	Capacity	0.5 MW
	α_i	0.95
System constraints	V^{min}	0.95p.u.
	V^{max}	1.05p.u.
	V_{sub}	1.05p.u.
	Peak fixed load	5.323 MW + j3.773 MVar
HVAC & EWH aggregator	Location	Bus #14, 18, 22, 33, 40, 45, 61
	Number of houses	200, 200, 200, 200, 200, 200, 200
	SOC limit	[0.15, 0.85]
	Ramp up/down rate	0.1
	Water mass m (kg)	144, 162, 180, 198, 216, 162, 180
	Heat loss H_r ($\times 10^{-2}$ kW)	5.6, 6.3, 7, 7.7, 8.4, 6.3, 7
	HVAC synchronization limit	[0.1, 0.7]
	EWH synchronization limit	[0, 0.7]
EV aggregator	Location	Bus #11, 21, 55, 64
	Number of EVs	300, 300, 300, 300
	Number of chargers	25, 25, 25, 25
	SOC limit	[0.2, 0.8]

6. Case studies

The proposed hybrid interval-stochastic tri-level model with multiple uncertainty sources is tested on a modified IEEE 69-bus distribution system. Simulations are performed on a laptop with an Intel Core i7-8650U CPU and 16 GB RAM. Problems are formulated in MATLAB R2020a and YALMIP and solved by GUROBI 9.0.0.

6.1. Modified IEEE 69-bus distribution system

The modified IEEE 69-bus system is shown in Fig. 2. Microturbines (MTs), static var compensators (SVCs), and PVs are installed in the
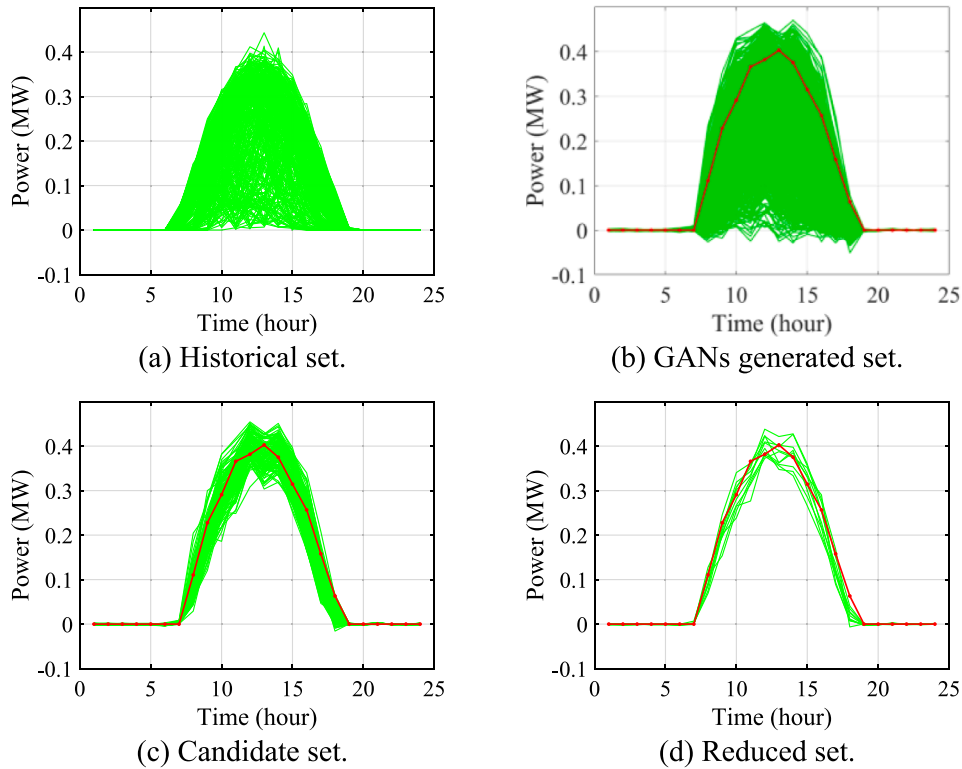
Fig. 3. PV power scenario sets.

Table 2
Aggregator payments and system generation cost under different uncertainty levels.

Case	Uncertainty level				Load aggregator payment ($)		System generation cost ($)	
	α^h	α^w	α^e	α^{temp}	Optimistic	Pessimistic	Optimistic	Pessimistic
1	0	0	0	0	999.00	999.00	3349.63	3349.63
2	0.001	0.01	0.01	0.005	985.08	1013.54	3335.71	3364.17
3	0.002	0.02	0.02	0.010	971.41	1028.25	3322.04	3378.88
4	0.003	0.03	0.03	0.015	958.18	1043.09	3308.81	3393.72
5	0.004	0.04	0.04	0.020	945.22	1058.08	3295.85	3408.71
6	0.005	0.05	0.05	0.025	932.62	1073.45	3283.25	3424.08
7	0.006	0.06	0.06	0.030	921.09	1088.94	3271.72	3439.57
8	0.007	0.07	0.07	0.035	910.65	1104.49	3261.29	3455.12
9	0.008	0.08	0.08	0.040	900.39	1120.38	3251.03	3471.01
10	0.009	0.09	0.09	0.045	890.35	1136.04	3240.98	3486.67
No flex	0	0	0	0	1529.71	1529.71	3850.27	3850.27

system. The parameters of the distribution system, HVAC aggregators, EWH aggregators, and EV aggregators are listed in Table 1.

For simplicity, it is assumed that each house has both HVAC and EWH, and if the owner is willing to participate in a LA, both HVAC and EWH are included. While the EV charging stations are located at some specific buses, they act as EV aggregators.

6.2. PV scenarios

The historical PV dataset is obtained from NREL Solar Integration Datasets [28]. The normalized power profiles over one year are illustrated in Fig. 3 (a). Based on GANs, 1200 PV power scenarios are generated as shown in Fig. 3 (b). These scenarios cover the most possible PV power outputs in one year, but they are not proper for the schedule of a specific day. Thus, according to Algorithm 1, 360 scenarios are selected as the candidate scenario set, which is shown in Fig. 3 (c). However, the candidate set still has too many scenarios. Then, they are further reduced, and finally 10 scenarios are kept, which are shown in Fig. 3 (d). In these figures, green curves are generated scenarios, and the

red curve is the forecasted day-ahead PV curve in a specific day.

If Fig. 3 (a) and Fig. 3 (b) are compared, we may observe that the scenarios generated by GANs can well follow the distribution of the historical set. From Fig. 3 (c) and Fig. 3 (d), it can be seen that the candidate set and the reduced set can cover the forecasted curve and maintain the ramp trend with the forecasted one. These findings demonstrate the power and effectiveness of GANs in scenario generation.

6.3. Day-ahead scheduling

The results of the DA scheduling are illustrated and discussed in this subsection. Table 2 shows the aggregator payments and system generation cost under different uncertainty levels. It can be observed that with the increase of the uncertainty level, the payments and cost increase in the pessimistic model and decrease in the optimistic model. This is because a bigger uncertainty level will worsen the worst operating condition for the pessimistic model while extending the feasible region for the optimistic model. Note that when the uncertainty scaler is too
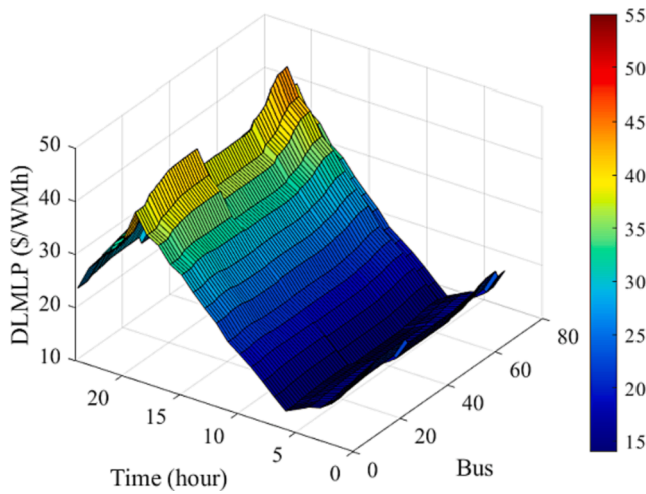
Fig. 4. Expected DLMP.

Table 3
DLMP and its components of one branch at $t = 19:00$.

Node	DLMP ($)	Energy ($)	Loss ($)	Voltage support ($)
1	41.240	41.24	0	0
2	41.242	41.24	0.002	0
3	41.244	41.24	0.004	0
4	41.249	41.24	0.009	0
47	41.251	41.24	0.011	0
48	41.298	41.24	0.058	0
49	41.447	41.24	0.207	0
50	41.468	41.24	0.228	0

*Energy, loss, voltage support refers to the three components of the DLMP.

large, like $\alpha^h \geqslant 0.05$, the pessimistic problem becomes infeasible, which indicates that the uncertainty level can affect the feasibility of the worst case.

The reason that α^h is less than α^w and α^e is that the indoor temperature is set to a tight range (e.g., [18, 22] ℃), thus a smaller α^h is proper. Also, a bigger α^h will easily make the indoor temperature exceeds the setting range due to the accumulative effect of the uncertainty which will further cause the problem infeasible.

The expected DLMP profile of the pessimistic model in Case 1 is illustrated in Fig. 4. Here, the expected DLMP is defined as the weighted

sum of the DLMP of all scenarios. At each time step, the DLMP varies spatially. This is because the marginal power loss price is a component of DLMP as stated in (36). Due to the radial topology, if there is no DG power injection, the DLMP increases when the node is farther away from node 1 because of a higher power loss factor at that node. The DLMP and its components of one branch (branch 1–2-3–4-47–48-49–50) at $t =$ 19:00 are shown in Table 3. Since no voltage constraints are violated, thus the voltage support price is $0.

At the same node, DLMP is lower during off-peak hours and higher during peak hours. This is because the wholesale market price is the main component of the DLMP, and thus DLMP has a similar pattern to the wholesale market price. With these characteristics, DLMP can be used to incentivize power consumption for flexible loads.

The system load profiles of the pessimistic model under different uncertainty levels are depicted in Fig. 5. In addition, the load profile of no flexible residential load is also depicted. Here, "no flexible load" means that residential loads do not response to the DLMP and are regarded as fixed loads. From Fig. 5, it can be observed that if compared with the Case "No flex", Case 1 ~ Case 10 have the load shifting effect, and Case 1 shifts the most load. The load shifting becomes weak as the uncertainty level increases.

The system load profiles of the optimistic model are depicted in Fig. 6. It can be found that all cases achieve the load shifting, and Case 10 is the best. Also, the electricity consumption decreases with the increase of uncertainty level. From Fig. 5 and Fig. 6, it can be concluded that bigger uncertainty level induces conservative results for the pessimistic model while radical results for the optimistic model.

6.4. Real-time scheduling

In this subsection, the optimistic results and the pessimistic results obtained by DA schedule and the results obtained by RT schedule are analyzed and discussed.

The flexible load profiles of the DA and RT schedules are shown in Fig. 7. For the pessimistic DA model, it can be found that during 5:00–13:00, the RT load curve is a bit higher than that of DA, while lower during 14:00–24:00. For the optimistic DA model, during 1:00–9:00, the RT load curve is somewhat overlapped with that of DA, while higher during 10:00–24:00. Overall, the optimistic DA schedule has the best load shifting effect, then the RT schedule and the pessimistic DA schedule. Such results are intuitive because the optimistic model represents the best ideal case, the pessimistic model represents the worst ideal case, and RT achieves a balance by modifying the two extreme cases by knowing more realistic operating information.
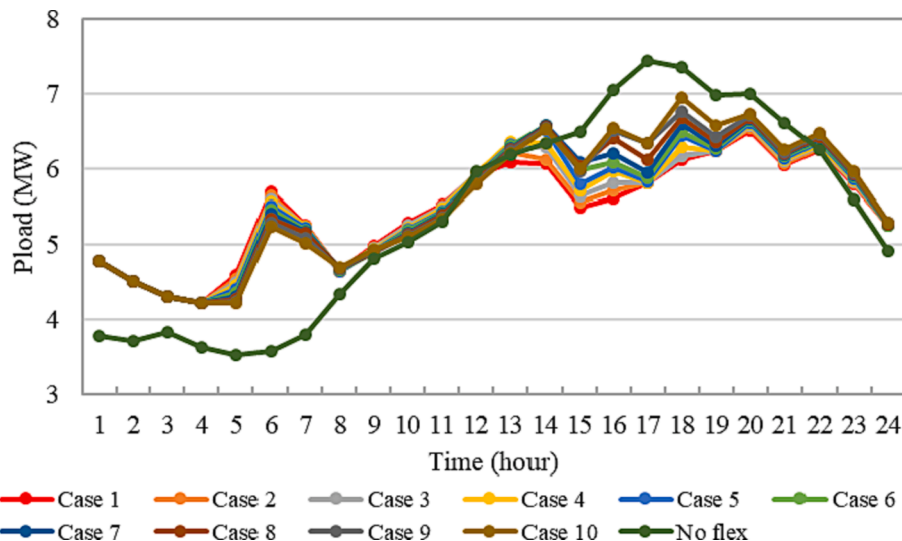

Fig. 5. System load profiles under different uncertainty levels for the pessimistic model.
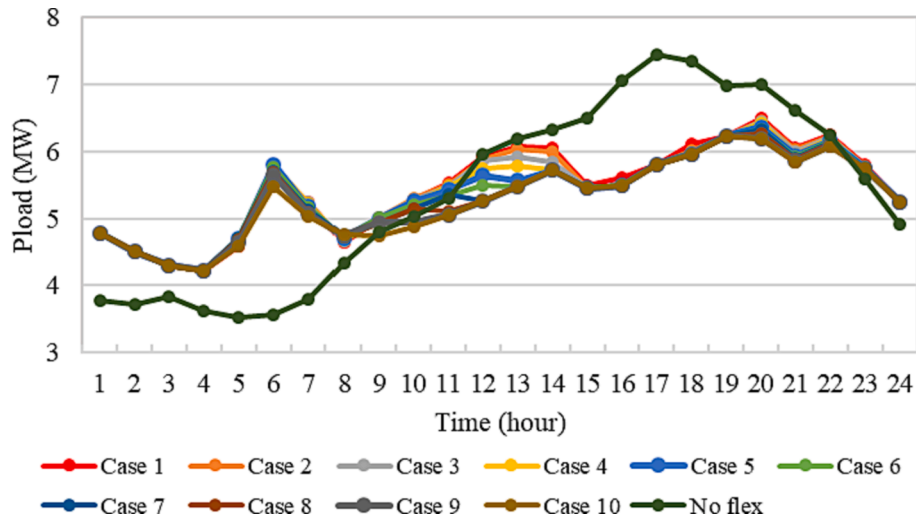
Fig. 6. System load profiles under different uncertainty levels for the optimistic model.
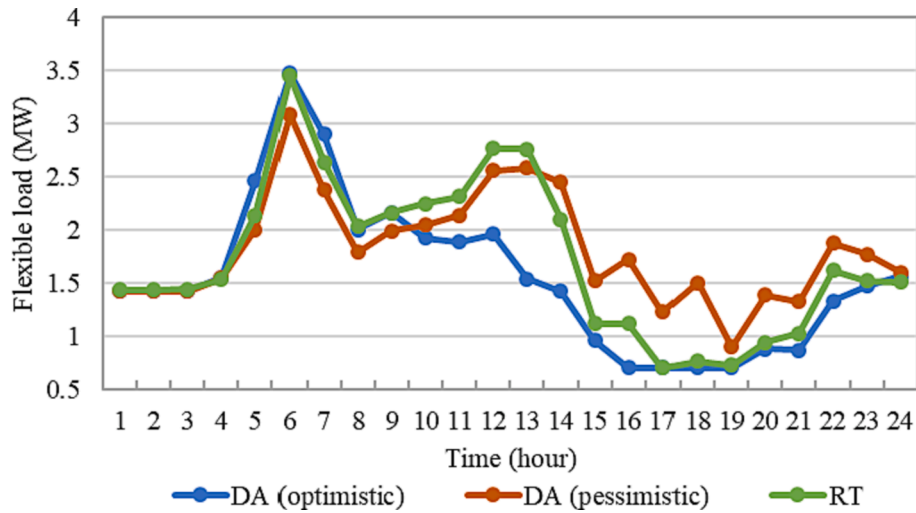

Fig. 7. Load profiles of total flexible load in day-ahead and real-time schedules.

The individual indoor temperatures in one HVAC aggregator in DA and RT are shown in Fig. 8 (a)(b)(c). The individual water temperatures in one EWH aggregator are shown in Fig. 8 (d)(e)(f).

From Fig. 8 (c), the HVAC indoor temperatures are just above the lower temperature set point during time intervals 40 ~ 80, and below the upper temperature set point during time intervals 115 ~ 144. This is exactly the precooling of HVACs and the DLMP plays an important role in forming these patterns. Incentivized by the temporal characteristic of the DLMP and the thermal storage characteristic of buildings, HVACs are turned on more frequently to cool down the building when the DLMP is low and are turned on less frequently to maintain the indoor temperature within the setting boundary when the DLMP is high. Water has a similar thermal storage characteristic due to its high specific heat capacity. Thus, water temperature shows similar patterns to the buildings' temperature. As shown in Fig. 8 (f), EWHs preheat water first and then maintain the water temperature within the setting range.

In addition, it can be observed that obviously, the individual indoor temperatures in the optimistic DA model usually exceed the setting temperature boundary, while the temperatures in the pessimistic model are mainly distributed in the middle of the temperature boundary, indicating the HVAC flexibility is either overused or underutilized. The temperatures in RT are well maintained inside or around the boundary, which means the precooling of HVACs is properly utilized. From Fig. 8

(d)(e)(f), water temperatures in RT are also better maintained in the setting boundary than that of DA.

These findings indicate that the day ahead scheduling is too radical or too conservative. The deployment of RHO by updating the operating information can significantly mitigate the radical or conservative DA scheduling.

7. Conclusion

In this paper, a three-layer market structure is established to quantitatively identify the flexibility potentials of residential buildings. In the day-ahead schedule, uncertainties from all layers are considered, which are the random power consumption behaviors, weather temperature forecasts, and PV power outputs. Then, a hybrid interval-stochastic programming is proposed, in which the Gaussian noise, interval forecast and GANs are utilized to model uncertainties respectively. In real-time, RHO is applied to continuously modify the day-ahead schedule according to the latest released information. Case studies have the following conclusions:

1) The trilevel structure can well utilize the residential demand flexibility to benefit individual users and satisfy their power needs, as well as reducing the distribution system total operational cost.
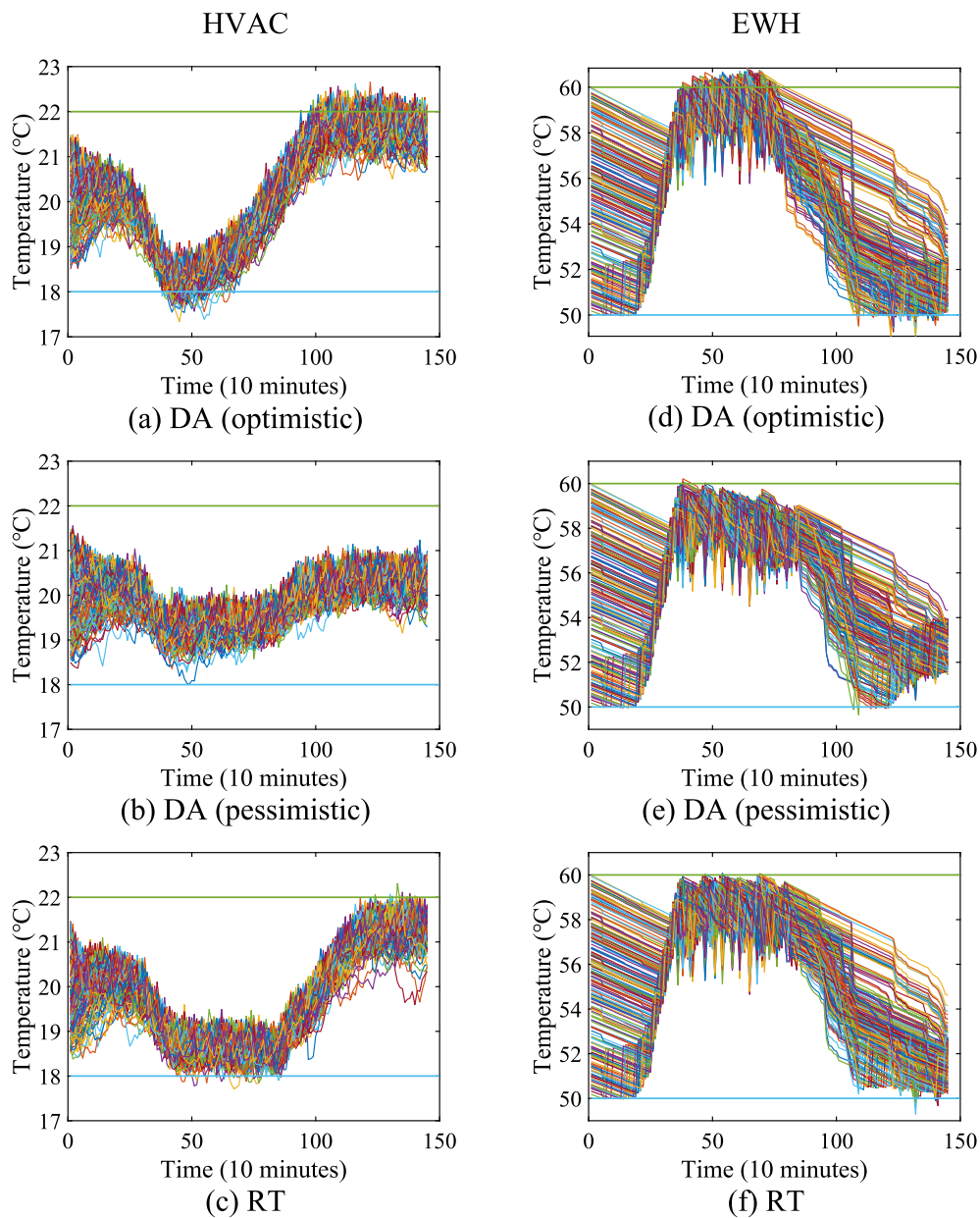
2) The proposed hybrid interval-stochastic programming can

Fig. 8. Indoor temperature profiles of HVACs and water temperatures of EWHs for 150 intervals of 10 min/interval.

effectively handle the uncertain bilevel problem and maintain the problem tractability. It can also provide optimistic and pessimistic results for decision-makers.

3) By integrating the latest system operating and forecast information, the RHO scheme can mitigate the radicalness and conservativeness of the day-ahead schedule.

CRediT authorship contribution statement

Xiaofei Wang: Conceptualization, Formal analysis, Methodology, Validation, Writing – original draft. **Fangxing Li:** Supervision, Funding acquisition, Conceptualization, Writing – review & editing. **Jin Zhao:** Validation, Writing – review & editing. **Mohammed Olama:**

Methodology, Writing – review & editing. **Jin Dong:** Methodology, Writing – review & editing. **Hang Shuai:** Validation, Writing – review & editing. **Teja Kuruganti:** Project administration, Funding acquisition.

Declaration of Competing Interest

The authors declare that they have no known competing financial interests or personal relationships that could have appeared to influence the work reported in this paper.

Data availability

The authors do not have permission to share data.

Appendix: Modeling of EWH

A single EWH can be modeled with the following expressions [29]:

$$\theta_{t+1}^w = a^w \theta_t^w - b^w W_t^D + g^w u_t^w + c^w \tag{49}$$

$$\theta^{w,\min} \leqslant \theta_t^w \leqslant \theta^{w,\max} \tag{50}$$

$$a^w = \left(1 - \frac{3600\Delta t H_r}{40 m c_p}\right) \tag{51}$$

$$c^w = \frac{3600 H_r \theta_t^h}{40 m c_p} \tag{52}$$

$$g^w = 3600 \cdot \frac{P^{w,rated}}{m c_p} \tag{53}$$

$$b^w = \frac{\left(\theta_t^w - \theta^{w,co}\right)}{m} \tag{54}$$

where $P^{w,rated}$ is the rated power of the heating element, m is the mass of the water inside the water tank, c_p is the specific heat of water (4.2 kJ/kg ℃), 3600 is to transfer time unit from hour to second, H_r represents the amount of water tank heat loss to the ambient per second, and $\theta^{w,co}$ is the temperature of inlet cold water. When obtaining b^w, it is assumed that the consumed hot water has a constant temperature of 55℃, since the used water temperature is always within the upper and lower limits. Typical parameters of an EWH are shown in Table 4.

Table 4
Parameters of a single EWH.

Parameter	Typical values
P^{rated}	3 (kW)
m	184 (kg)
H_r	0.07 (kW)
θ^{co}	10 (℃)
W^D	L/h
θ^{max}	60 (℃)
θ^{min}	50 (℃)
Δt	1 h

Note, the indoor temperature θ_t^h is assumed constant (20℃) in this model because it fluctuates within a tight range due to the HVAC in the house, and $\theta_t^{w,co}$ is also assumed constant (10 ℃).

References

[1] Satchwell A, et al. A national roadmap for grid-interactive efficient buildings. Berkeley, CA, USA: LBNL; May 2021.

[2] Liu G, Tao Y, Xu L, Chen Z, Qiu J, Lai S. Coordinated management of aggregated electric vehicles and thermostatically controlled loads in hierarchical energy systems. Int J Electr Power Energy Syst 2021;131:107090.

[3] Li H, Wang Z, Hong T, Piette MA. Energy flexibility of residential buildings: A systematic review of characterization and quantification methods and applications. Advances in Applied Energy 2021;3:100054.

[4] Rastogi D, Lehner F, Kuruganti T, Evans KJ, Kurte K, Sanyal J. The role of humidity in determining future electricity demand in the southeastern United States. Environ Res Lett 2021;16(11):114017.

[5] Yuan H, Li F, Wei Y, Zhu J. Novel linearized power flow and linearized OPF models for active distribution networks with application in distribution LMP. IEEE Trans Smart Grid Jan. 2018;9(1):438–48.

[6] Kou X, et al. A scalable and distributed algorithm for managing residential demand response programs using alternating direction method of multipliers (ADMM). IEEE Trans Smart Grid June 2020;11(6):4871–82.

[7] Shi Q, Chen C, Mammoli A, Li F. Estimating the profile of incentive-based demand response (IBDR) by integrating technical models and social-behavioral factors. IEEE Trans Smart Grid Jan. 2020;11(1):171–83.

[8] Conte F, et al. Performance analysis of frequency regulation services provided by aggregates of domestic thermostatically controlled loads. Int J Electr Power Energy Syst 2021;131:107050.

[9] Wang X, et al. Tri-level scheduling model considering residential demand flexibility of aggregated HVACs and EVs under distribution LMP. IEEE Trans Smart Grid Sep. 2021;12(5):1949–3053.

[10] Park B, Chen Y, Olama M, Kuruganti T, Dong J, Wang X, et al. Optimal demand response incorporating distribution LMP with PV generation uncertainty. IEEE Trans Power Syst 2022;37(2):982–95.

[11] Patnam BSK, Pindoriya NM. DLMP calculation and congestion minimization with EV aggregator loading in a distribution network using bilevel program. IEEE Syst J June 2020;15(2):1835–46.

[12] Yi Z, Xu Y, Zhou J, Wu W, Sun H. Bi-level programming for optimal operation of an active distribution network with multiple virtual power plants. IEEE Trans Sustain Energy Oct. 2020;11(4):2855–69.

[13] Quashie M, Bouffard F, Marnay C, Jassim R, Joós G. On bilevel planning of advanced microgrids. Int J Electr Power Energy Syst 2018;96:422–31.

[14] Karimi H, Bahmani R, Jadid S. Stochastic multi-objective optimization to design optimal transactive pricing for dynamic demand response programs: A bi-level fuzzy approach. Int J Electr Power Energy Syst 2021;125:106487.

[15] Cui S, Wang Y, Xiao J, Liu N. A two-stage robust energy sharing management for prosumer microgrid. IEEE Trans Ind Informat Aug. 2018;15(5):2741–52.

[16] Kou X, Du Y, Li F, Pulgar-Painemal H, Zandi H, Dong J, et al. Model-based and data-driven HVAC control strategies for residential demand response. IEEE Open Access Journal of Power and Energy 2021;8:186–97.

[17] Ma K, et al. Hybrid control of aggregated thermostatically controlled loads: Step rule, parameter optimisation, parallel and cascade structures. IET Gener, Transm Distrib, Dec 2016;10(16):4149–57.

[18] M. Vahid-Ghavidel et al., "Novel hybrid stochastic-robust optimal trading strategy for a demand response aggregator in the wholesale electricity market," *IEEE Trans. Ind. Appl.*, vol. 57, no.5, pp. 5488-5498, Sept.-Oct. 2021.

[19] Kou X, Li F. Interval optimization for available transfer capability evaluation considering wind power uncertainty. IEEE Trans Sustain Energy Jan. 2020;11(1): 250–9.

[20] Zheng Z, Sun Z, Pan J, Luo X. An integrated smart home energy management model based on a pyramid taxonomy for residential houses with photovoltaic-battery systems. Appl Energy 2021;298:117159.

[21] Stappers B, Paterakis NG, Kok K, Gibescu M. A class-driven approach based on long short-term memory networks for electricity price scenario generation and reduction. IEEE Trans Power Syst July 2020;35(4):3040–50.

[22] Chen Y, Wang Y, Kirschen D, Zhang B. Model-free renewable scenario generation using generative adversarial networks. IEEE Trans Power Syst May 2018;33(3): 3265–75.

[23] Dupačová J, Gröwe-Kuska N, Römisch W. Scenario reduction in stochastic programming. Math Program Feb. 2003;95(3):493–511.

[24] Wang X, Li F, Zhang Q, Shi Q, Wang J. Profit-oriented BESS siting and sizing in deregulated distribution systems. *IEEE Trans Smart Grid*, early access 2022.

[25] Sinha A, Malo P, Deb K. A review on bilevel optimization: From classical to evolutionary approaches and applications. IEEE Trans Evol Comput April 2018;22 (2):276–95.

[26] Conejo AJ, Ruiz C. Complementarity, Not Optimization, is the Language of Markets. IEEE Open J Power Energy 2020;7:344–53.

[27] Palma-Behnke R, Benavides C, Lanas F, Severino B, Reyes L, Llanos J, et al. A microgrid energy management system based on the rolling horizon strategy. IEEE Trans Smart Grid June 2013;4(2):996–1006.

[28] NREL., Solar Integration National Dataset Toolkit, [Online] Available: https:// www.nrel.gov/grid/sind-toolkit.html.

[29] Bozchalui MC, Hashmi SA, Hassen H, Canizares CA, Bhattacharya K. Optimal operation of residential energy hubs in smart grids. IEEE Trans Smart Grid Dec. 2012;3(4):1755–66.